DRAFT VERSION FEBRUARY 17, 2009
Preprint typeset using LaTeX style emulateapj

STELLAR-MASS BLACK HOLE SPIN CONSTRAINTS FROM DISK REFLECTION AND CONTINUUM MODELING

J. M. MILLER[1], C. S. REYNOLDS[2], A. C. FABIAN[3], G. MINIUTTI[3,4,5], L. C. GALLO[6]

Subject headings: Black hole physics – relativity – stars: binaries

Draft version February 17, 2009

ABSTRACT

Accretion disk reflection spectra, including broad iron emission lines, bear the imprints of the strong Doppler shifts and gravitational red-shifts close to black holes. The extremity of these shifts depends on the proximity of the innermost stable circular orbit to the black hole, and that orbit is determined by the black hole spin parameter. Modeling relativistic spectral features, then, gives a means of estimating black hole spin. We report on the results of fits made to archival X-ray spectra of stellar-mass black holes and black hole candidates, selected for strong disk reflection features. Following recent work, these spectra were fit with reflection models and disk continuum emission models (where required) in which black hole spin is a free parameter. Although our results must be regarded as preliminary, we find evidence for a broad range of black hole spin parameters in our sample. The black holes with the most relativistic radio jets are found to have high spin parameters, though jets are observed in a black hole with a low spin parameter. For those sources with constrained binary system parameters, we examine the distribution of spin parameters versus black hole mass, binary mass ratio, and orbital period. We discuss the results within the context of black hole creation events, relativistic jet production, and efforts to probe the innermost relativistic regime around black holes.

1. INTRODUCTION

X-rays probe the innermost regime around compact objects. Modern data aside, this must hold true based on simple theoretical considerations. Temperature relations for standard blackbody accretion disks and the energy budget of scattered emission that might account for hard X-ray production both demand that X-ray emission arise close to compact objects. Thus, the promise of X-ray studies of black holes is that it may allow observers to study the innermost regime, and so explore general relativity in the strong field limit. The promise is especially rich in the case of stellar-mass black holes, because the disk is itself an X-ray object, and spectra are not complicated by a stellar surface and boundary layer as in the case of neutron stars.

Measuring spin in stellar-mass black holes can do more than confirm the predictions of the Kerr metric. Unlike supermassive black holes in galactic centers, stellar-mass black holes likely gain most of their angular momentum at the moment of their birth (Volonteri et al. 2005, Gammie et al. 2004). Spin is therefore a window into the nature of the supernovae and/or gamma-ray bursts that give rise to stellar-mass black holes (many progenitor star properties are important; see Heger & Woosley 2002). Some models for jet production in black holes rely on tapping the spin energy of the hole, and so predict a link between spin and jets (e.g. Blandford & Znajek 1977). In the case of AGN, radio loudness is often used as a proxy for spin (see, e.g., Sikora, Stawarz,& Lasota 2007); this proxy creates a circularity in efforts to understand jet production mechanisms. While the sample of AGN is much larger than the sample of stellar-mass black holes in the Milky Way, the proximity of stellar-mass black holes facilitates direct investigations of spin that can bear on jet mechanisms.

Iron emission lines formed in the inner accretion disk will bear the imprints of the strong Doppler shifts and gravitational red-shifts endemic to that region, and so can serve as incisive probes of the innermost relativistic regime (for a review, see Miller 2007). A major advantage of disk lines is that the mass of the black hole is not required to make a spin measurement, and other parameters – such as the inner disk inclination – can be measured directly. In recent years, these lines (and the larger disk reflection spectrum, of which iron lines are the most prominent part) have been used to obtain general constraints on black hole spin. (The dimensionless spin parameter is given by $a = cJ/GM^2$ and values range from zero to one). For instance, line profiles in XTE J1650–500 and GX 339–4 could be fit well with a model appropriate for a disk around a maximally-spinning black hole (Miller et al. 2002, Miniutti, Fabian, & Miller 2004, Miller et al. 2004a, 2006; Laor 1991).

It is only within the last two years that fits to spectra have started to yield non-zero spin constraints that could properly be called measurements. A spin of $a > 0.98$ has been reported for the Seyfert-1 AGN MCG-6-30-15 (Brenneman & Reynolds 2007), and a spin of $a = 0.93(5)$ has been reported in GX 339-4 (Miller et al. 2008; see also Reis et al. 2008). This advance is partly due to improved spectra and partly due to the development of new, variable-spin line models. It is now clear that relativistic disk lines are also present in neutron star spectra (see, e.g., Bhattacharyya & Strohmayer 2008, Cackett et al. 2008), providing a means of constraining fundamental neutron star parameters and a useful comparison for black hole spectra.

The accretion disk continuum can, in principle, also be ex-

[1]Department of Astronomy, University of Michigan, 500 Church Street, Ann Arbor, MI 48109, jonmm@umich.edu
[2]Department of Astronomy, The University of Maryland, College Park, MD, 20742
[3]Institute of Astronomy, University of Cambridge, Madingley Road, Cambridge CB3 OHA, UK
[4]Laboratoire APC, UMR 7164, 10 rue A. Domon et L. Duquet, 75205 Paris, FR
[5]LAEX, Centro de Astrobiolgia (CSIC-INTA), LAEFF, P.O. Box 78, E–28691, Villanueva de la Cañada, Madrid, ES
[6]Department of Astronomy & Physics, Saint Mary's University, 923 Robie Street, Halifax NS B3H 3C3

ploited to constrain black hole spin. Especially in the case of stellar-mass black holes, wherein the disk is an X-ray object and can dominate the total spectrum, this method is promising. The development of new disk models, supported by numerical disk simulations, has enabled spin constraints in a few systems based on the thermal continuum emission from the disk (Shafee et al. 2006, McClintock et al. 2006). This method essentially amounts to measuring the emitting area of the accretion disk, and so requires accurate knowledge of a given black hole mass, its distance, and a detector with an accurate flux calibration.

Quasi-periodic oscillations (QPOs) in the X-ray flux of accreting compact objects may provide an incisive way of studying orbital motion near to black holes (for a review, see van der Klis 2006). A number of difficulties persist, however. The high frequency (100 Hz and above) QPOs that are most plausibly associated with inner orbits around black holes are too hard (spectrally) to arise via direct emission from the accretion disk (see, e.g., Homan et al. 2001). Moreover, shifts in QPO frequencies are not easily interpreted as due to changes in the inner edge of the disk as they can occur at high mass accretion rates where the disk must be at its innermost stable circular orbit (ISCO). Frequencies and frequency changes may have a complex dependence on a combination of the inner disk radius, mass accretion rate, and other paramters (see, e.g., van der Klis 2001). At present, there is no theory that can fully explain the frequencies observed, how such frequencies might arise, and their energy budget (for a discussion, see Reynolds & Miller 2008).

It is now possible to make a systematic spectral analysis of spin in stellar-mass black holes that exploits all of the best, most physically-motivated models. We have identified a set of eight stellar-mass black holes and black hole candidates, selected for having strong, broad iron lines. Whenever possible, data from CCD spectrometers was used in order to take advantage of moderate spectral resolution. In order to construct the most self-consistent models possible, we fit all of the spectra with blurred disk reflection models and disk continuum models in which spin is a variable. In each case, the spin parameter in the disk continuum and blurred disk reflection models were linked, in order to obtain the most robust constraints possible. In the sections that follow, we detail aspects of the source sample, our analysis methods, the results of our analysis, sources of systematic errors and biases, and possible implications.

2. OBSERVATIONS AND DATA REDUCTION

Optical and infrared observations have constrained the properties of six of the eight binary systems in our sample. The parameters of these systems are reported in Table 1. In some cases, such as GRO J1655–40, values have been measured precisely; however, this is not typical. The numbers quoted in Table 1 reflect our best estimates of the value and uncertainty in each parameter of interest. Where uncertainties are a large fraction of the value itself, a range is given instead of a value and associated error.

2.1. *4U 1543–475*

We analyzed the very high state spectrum with the largest line equivalent width, as measured by Park et al. (2004). This observation was made on 2002 July 19, and is archived as 70133-01-29-00. The *RXTE* standard products from the archive were utilized. These files include source and background spectra as well as instrument responses. The standard PCA source spectrum is a sum of all layers from PCU-2 and PCU-3. The HEXTE cluster-B spectrum was analyzed jointly with the PCA spectrum. The net exposures were 1.1 ksec and 0.4 ksec for the PCA and HEXTE, respectively.

We followed standard practices in fitting the PCA and HEXTE spectra. We added 0.6% systematic errors to the PCA spectrum using the ftool "grppha". Within XSPEC, the PCA spectrum was fit in the 2.8–25.0 keV range, and the HEXTE spectrum was fit in the 20.0–50.0 keV range. The upper limit for the HEXTE spectrum is the highest energy at which the source is confidently detected. All fitting parameters were linked between the PCA and HEXTE spectra; an overall normalizing constant allowed to float between the spectra.

2.2. *XTE J1550–564*

The best available disk reflection spectra of XTE J1550–564 were obtained with *ASCA* during the 1998 outburst. We analyzed the *ASCA*/GIS spectra previously discussed in Miller et al. (2005). These spectra were accumulated on 1998 September 23 in the very high state; a net exposure of 25 ksec was obtained. The standard source and background files and responses from the *ASCA* standard products (available through HEASARC) were analyzed. The reduction of these data follows the method best suited to bright sources, outlined by Brandt et al. (1996).

We fit the GIS-2 and GIS-3 spectra jointly in the 1–10 keV band. The spin parameter, inner disk inclination, reflection fraction, and ionization parameter were linked in joint fits to the spectra, and linked between model components where appropriate. Other parameters relevant to the continuum were allowed to float. This is a pragmatic approach driven by the fact that different cameras, even on the same observatory, never have perfectly consistent flux calibrations. For clarity and simplicity, the parameters measured from GIS-2 are reported in Table 2 and Table 3.

2.3. *XTE J1650–500*

At present, the mass of this black hole has not been precisely determined, but preliminary constraints have been made (see Orosz et al. 2004). In this work, we assume a mass range 3–7 $M_{\odot}$ for the black hole. The upper mass limit is based on an assumed mass ratio of $q \simeq 10$ (Orosz et al. 2004). A mass ratio of $q = 10$ is therefore assumed in this work, and we attach fiducial errors of 30% to be conservative. XTE J1650−500 was observed with *XMM-Newton* on 2001 September 13. We analyzed the same EPIC-pn spectrum discussed in Miller et al. (2002). The spectrum was accumulated over 21 ksec. The spectral parameters reported by Miller et al. (2002) and Miniutti, Fabian, & Miller (2004), especially when viewed in the context of the extensive work done by Rossi et al. (2005), suggest the source was in a rising phase of the low/hard state when observed with *XMM-Newton*.

Owing to calibration uncertainties in pn "burst" timing mode, we restricted our fits to the 0.7–10.0 keV range. This range was also used in recent fits to the EPIC-pn "burst" mode spectrum of GX 339–4 in the very high state (Miller et al. 2004, 2008). A Gaussian with zero width was included at 2.3 keV to account for calibration uncertainties in that range. Imperfect modeling of silicon features and gold features continue to have small effects in the 2–3 keV range in "burst" mode. These narrow-band calibration problems do not affect results related to the continuum, iron line, or reflection.

2.4. *GRO J1655–40*

Although the fundamental parameters of this binary are known precisely, GRO J1655−40 is a challenging source. The rich absorption spectrum observed in some very high and high/soft states of GRO J1655−40 (e.g. Miller et al. 2006b, Diaz Trigo et al. 2007, Miller et al. 2008b) can serve to complicate disk reflection spectroscopy. Absorption lines from Fe XXV and Fe XXVI fall in the midst of the relativistic Fe disk line. Prior claims for strong Doppler-shifted emission lines by Balucinska-Church and Church (2000), for instance, might be partially explained by an absorption line amidst a broad emission line.

A spectrum with a strong power-law component (for constrast) and little absorption is optimal for spin constraints. Archival spectra of bright states obtained with *ASCA*, *Chandra*, and *XMM-Newton* are all complicated by absorption. A recent observation of GRO J1655−40 in the low/hard state with *Suzaku* does not find an Fe disk line (Takahashi et al. 2008); improved calibration may enable more detailed studies in the future. Thus, although a focusing telescope and CCD resolution are strongly preferred, we turned to *RXTE*. The large number of observations that *RXTE* executes makes it possible to find a more suitable spectrum.

RXTE observed GRO J1655−40 during its outburst in 1996. Sobczak et al. (1999) made fits to these spectra. We selected the very high state observation with the strongest power-law flux, for best overall contrast. Sobczak et al. (1999) do not find evidence for absorption in these spectra, and the power-law index was found to be reasonably hard ($\Gamma = 2.64$).

As with 4U 1543−475, the standard products (source and background files, and response files) from the public archive were analyzed. The spectra were obtained on 1996 November 2; net exposures of 4.9 ksec and 1.6 ksec were recorded with the PCA and HEXTE, respectively. We added 0.6% errors to the PCA spectrum using "grppha". All fit parameters between the PCA and HEXTE spectra were linked, apart from an overall normalizing constant that was allowed to float between them.

2.5. *GX 339–4*

GX 339−4 is a recurrent Galactic black hole binary that has undergone numerous outbursts. At the time of writing, it is the only black hole that has been observed in *every* outburst state with CCD and/or dispersive X-ray spectrometers. While the orbital period of GX 339−4 is well known, the mass of the companion star is not. Hynes et al. (2003) and Munoz-Darias et al. (2008) have independently tried to estimate the mass of the black hole in GX 339−4. For the purposes of this analysis, we adopt conservative values from these analyses: $M_{BH} \geq 6\ M_{\odot}$ and $q \geq 8$.

It is difficult to obtain the black hole mass precisely because light from the accretion disk "contaminates" light from the companion even in quiescent phases in GX 339−4, complicating measurements of its inclination. Constraints derived from jet flux ratios in this system strongly suggest a low inclination for the inner disk (e.g., $\theta \leq 30^{\circ}$, see Gallo et al. 2004 and Miller et al. 2004). The inclination of the inner disk may be lower than the inclination of the binary. The inclination was a free parameter in all fits reported in this work.

We fit the same very high state spectrum detailed in Miller et al. (2004) and Miller et al. (2008). This EPIC-pn "burst" mode spectrum was obtained on 2002 September 29; a 75.6 ksec exposure was recorded. Prior analysis of the disk line and disk reflection spectrum in GX 339−4 suggests a black hole spin parameter of $a = 0.93 \pm 0.05$ (Miller et al. 2008, Reis et al. 2008). These measurements draw on multiple excellent spectra and appear to be independent of the disk reflection model used; they are likely to be fairly robust. However, prior modeling efforts made use of more phenomenological models for the thermal disk continuum. While the more physical disk continuum model used in this work does not give a statistically superior description of the disk spectrum in GX 339−4, it is more physical. As with other "burst" mode spectra, we fit the spectrum of GX 339−4 over the 0.7–10.0 keV range.

2.6. *SAX J1711.6–3808*

SAX J1711.6−3808 was observed in outburst as a moderately-bright transient in 2001. The parameters of the binary system have not yet been constrained. Observations made by *BeppoSAX* and *RXTE* are reported by in 't Zand (2002) and Wijnands & Miller (2002). The source was observed by *XMM-Newton* and a relativistic iron line has been reported (Sanchez-Fernandez et al. 202, AN, 327, 1004), but the spectrum is complicated by photon pile-up and so excluded from our analysis.

We analyzed the *BeppoSAX* MECS spectrum previously examined by in 't Zand et al. (2002). The source was observed with the MECS starting on 2001 February 16. A net exposure of 37 ksec was obtained. We fit the single MECS spectrum in the 2-10 keV range. Thermal disk emission was not detected in this spectrum. This is likely due in part to the relatively high line of sight absorption ($N_H = 2.57(7) \times 10^{22}$ cm^{-2}), which would be especially effective in hiding a cool disk (see, e.g., Miller et al. 2006). The hard power-law index and lack of a hot disk component strongly suggest that SAX J1711.6−3808 was observed in the low/hard state. Parameters such as the black hole mass and distance are not required in disk reflection fits; the inner disk inclination was allowed to vary freely.

2.7. *XTE J1908+094*

Like SAX J1711.6−3808, XTE J1908+094 was observed as a moderately bright transient with characteristics typical of black hole systems. At present, the parameters of this binary system are unknown.

We analyzed the *BeppoSAX* MECS spectra previously examined by in 't Zand et al. (2002b). The source was observed starting on 2002 April 2 for a total of 56.6 ksec. XTE J1908+094 was found to be highly variable during this time, so in 't Zand et al. (2002b) examined seven spectra from different time slices. To facilitate comparisons with this prior work, we followed the same procedure. The same spectra were fit jointly in the 2–10 keV band. Quantities such as power-law index and flux were allowed to float between observations, but the disk reflection parameters and spin parameters were linked. As with SAX J1711.6−3808, thermal emission from the disk was not detected, likely due to a combination of high line-of-sight absorption and the expectation of an intrinsically cool disk in the low/hard state. Here again, the current lack of constraints on the system parameters poses no difficulty for disk reflection modeling. The inclination and other parameters were allowed to vary freely in all fits.

2.8. *Cygnus X-1*

Efforts to measure the parameters of this binary system are complicated by the fact that the companion is an O9.7 Iab supergiant, and by the fact that the system is persistently active. As the inclination is poorly known, this parameter was allowed to float freely in all spectral fits.

We analyzed two *XMM-Newton*/EPIC-pn spectra of Cygnus X-1 in its "high" state. It should be noted that the "high" state in Cygnus X-1 is an archaic label; the same phase is called the "very high" state in other sources. These spectra were obtained in "burst" timing mode, like the spectrum of XTE J1650–500. Preliminary fits to one of these spectra are discussed in Miller et al. (2007). The spectra were obtained on 2004 October 6 and 2004 October 8; a net exposure of 0.5 ksec were obtained in each case. This is relatively short; however, the proximity of Cygnus X-1 and its high flux state when observed yielded sensitive spectra. Events were extracted using a narrow strip along the full height of the DETX-DETY plane. Spectral files were produced by selecting event grades 0–4 and enforcing "FLAG=0" within "xmmselect". Spectral channels 0–20,479 were grouped by 5 as required for pn analysis. The "rmfgen" and "arfgen" tools were used to create response files. As with other "burst" mode spectra, we fit the spectra of Cygnus X-1 on the 0.7–10.0 keV band. The spectra were fit jointly. The spin parameters were linked, but as the spectra were not simultaneous all other parameters were allowed to vary independently. For clarity and convenience, the result of fits to the first observation are listed in Table 2 and Table 3.

In the fits described below, we allowed for a narrow Gaussian absorption line corresponding to Fe XXV or Fe XXVI to account for any absorption in the massive companion wind. The width of the Gaussian was fixed to zero, as wind velocities are below the resolution of the detector. The addition of such a line gave only marginal improvements, and equivalent widths of approximately 30 eV and 10 eV for the first and second observations, respectively.

2.9. *Conspicuous Absentees*

GRS 1915+105 is an important but complex source requiring individual treatment, and so it has been left out of this analysis. Prior fits to the disk line in this source did not require black hole spin; indeed, the fits were suggestive of a low spin parameter (Martocchia et al. 2002). More recent fits to the thermal continuum have suggested a near-maximal spin (McClintock et al. 2006). More work is needed to resolve this disparity. The results of disk reflection modeling of a recent *Suzaku* spectrum of GRS 1915+105 will be reported by Blum et al. (2009).

Iron emission lines are evident in the spectra of V4641 (in 't Zand 2000), and those lines can indeed be modeled as relativistic disk lines (Miller et al. 2002b). However, it is not clear that iron lines can be used to study the inner accretion flow in this source. Emission lines from the inner disk may be contaminated by lines from a surrounding nebula or outflow. This possibility was first recognized by Revnivtsev et al. (2002) based on observations made in outburst. More recent *Chandra* observations of the source in a nearly quiescent flux state also reveal iron emission lines (Gallo et al. 2009).

3. ANALYSIS AND RESULTS

3.1. *Models and Methodology*

Using the inner disk as an indirect measure of the black hole spin parameter depends on two assumptions; firstly, that the accretion flow has a sharp transition from turbulent orbital flow to an inward plunging flow at (or close to) the innermost stable circular orbit; and second that the iron line emission has an inner truncation radius due to this transition in the flow properties. Recent 3-dimensional magnetohydrodynamic simulations of black hole disks suggest that these assumptions are valid if the disk is sufficiently thin (Reynolds & Fabian 2008; Shafee et al. 2008). This condition likely holds for the range of outburst phases covered in this work, including relatively low accretion rates in the low/hard state (see Miller et al. 2006b; Rykoff et al. 2007). Therefore, in selecting spectra for this analysis, bright phases of the low/hard state are taken to be as relevant and well-suited as observations made in brighter states.

All spectra were fit using XSPEC version 11.3 (Arnaud & Dorman 2000). The spectra from each source were fit with a model consisting of the "kerrbb" thermal disk continuum model (Li et al. 2005; this is the same model employed by Shafee et al. 2006 and McClintock et al. 2006) and the constant density ionized (CDID) disk reflection model (Ballantyne, Ross, & Fabian 2001). This reflection model is calculated in the fluid frame. To translate this spectrum into that seen by a distant observer, we convolved the CDID model with the "kerrconv" model (Brenneman & Reynolds 2006). "Kerrconv" encodes the Doppler and gravitational shifts expected close to a black hole, as a function of the black hole spin parameter. Convolving a reflection spectrum is more physically self-consistent than merely treating the relativistic line, because the line and broad-band reflection spectrum are produced in the same physical location through the same process.

The black hole spin parameter a and inner disk inclination θ are common to the "kerrbb" and "kerrconv" models. These parameters were linked in fits to each spectrum of a given source, and linked in spectra from different observations of the same source. That is, the disk reflection and continuum spectra *jointly* determined the spin parameter and inner disk inclination in our fits. For the two sources where thermal emission from the disk was not detected, spin constraints were obtained through the disk reflection spectrum alone.

Apart from the black hole spin parameter and the inner disk inclination, important parameters in the "kerrconv" model inlcude the inner disk radius (in units of the ISCO) and the reflection emissivity index. The inner radius was fixed at 1.0; this amounts to assuming that the disk is at the ISCO. The emissivity is taken to be a power-law in radius of the form $J(r) \propto r^{-q}$. A simple lamp-post model gives $q = 3$. While prior work assumed this form partially for simplicity, recent microlensing observations provide an interesting physical justification (Chartas et al. 2008). Other results have found steeper emissivity indices, perhaps suggesting that the hard component is anisotropic (Miniutti & Fabian 2004). This may be consistent with hard X-ray emission in the base of a jet. Whatever the proper physical picture, this parameter is one that can be directly constrained by data. In all fits, the emissivity index was constrained to be in the range $3 \leq q \leq 5$; this range is commensurate with that found in the literature (see, e.g., Miller et al. 2007).

The CDID disk reflection model is capable of handling a broad range of disk ionization, including high ionization states. The ionization parameter is used to express a ratio of flux to gas density: $\xi = L_X/nr^2$, where n is the hydrogen number density. This is important in X-ray binaries; reflection occurs in the upper levels of the disk, not the midplane, and that region is expected to be highly ionized. Results reported in the literature vary between $\log(\xi) = 3$ and $\log(\xi) = 5$, depending on the source state and luminosity (see Miller 2007). This range defines the bounds adopted in our fits. While this model does not include thermal emission from the disk midplane, it appears that neglecting this does not markedly change the spin parameter obtained (see Miller et al. 2008 and Reis et al. 2008).

The CDID model can be applied as a "pure" reflection model, with no hard power-law flux included, but we employed a version that includes a power-law continuum flux. Important parameters in the CDID model that must be constrained include: the photon power-law index (the steepest power-law index possible is $\Gamma = 3$), the disk ionization parameter, the disk reflection fraction ($0 \leq R \leq 2$), and an overall normalizing factor. The normaliztion does not account for distance dilution and is a small number. The CDID model is an angle-averaged model: the inner disk inclination is not a variable that can be constrained by fitting. The version of the model that we used assumes solar abunances for all elements. To obtain good fits at the limits of a bandpass when using a convolved reflection model, it is necessary to extend the range over which the model is calculated within XSPEC using the "extend" command.

The "kerrbb" model has 10 parameters, including the black hole spin parameter and the inner disk inclination (Li et al. 2005). The full parameter list includes: the ratio of power due to torque at the ISCO to power arising from accretion (fixed to zero in all fits as per a Keplerian disk); the mass of the black hole in units of solar masses (constrained to lie in the ranges indicated in Table 1); the mass accretion rate through the disk (allowed to float in all fits); the distance to the black hole in units of kpc (constrained to lie in the ranges indicated in Table 1); the spectral hardening factor, a multiplicative factor accounting for radiative transfer through the disk atmosphere (the default value of 1.7 was assumed in all fits); a switch controlling self-irradiation (all fits neglected self-irradiation as per the default); a switch controlling limb darkening (turned off in all fits as per the default); and the overall model normalization. If all of the system parameters were known precisely, the normalization should be set to unity. In practice, the normalization serves to absorb difficulties with the system parameters, the flux calibration of the detector used, and other effects (see, e.g., Zimmerman et al. 2005).

To understand the influence of the disk continuum in estimating spin parameters, we also made independent fits with the "diskbb" model (Mitsuda et al. 1984) taking the place of the "kerrbb" model. This model has only two parameters, the color temperature of the inner disk and a flux normalization parameter. Three aspects of this model make it powerful: it is simple, and thus easily reproducible; it fits thermal spectra extremely well; and it has a long history in the literature, facilitating useful comparisons. Important physics, such as a zero-torque inner boundary condition and the effects of radiative transfer effects, are not included in the "diskbb" model.

3.2. *Spectral Fitting Results*

The results of our spectral fits are detailed in Table 2 and Table 3. Figures 1–16 depict fits to the spectra of each source with a simple continuum model (in order to highlight the disk reflection features), and fits made with the fully relativistic, physical models from which spin parameters are inferred (those described in Table 2). A histogram of the spin values listed in Table 2 is shown in Figure 17. The fits are imperfect; in many cases, they are not formally acceptable in a statistical sense. Where fits are not formally acceptable, the fit statistic is driven to unacceptable values mostly by instrumental features (see, e.g., Miller et al. 2004, for a discussion of features in the response of the *XMM-Newton*/EPIC-pn camera when operated in burst mode). It is clear in Figures 1–16 that the relativistic, physical models account for the disk reflection features very well.

Fits to the spectra of GRO J1655–40 and GX 339–4 suggest spin parameters of $a = 0.98(1)$ and $a = 0.94(2)$ respectively (1σ statistical errors). XTE J1650–500 and XTE J1550–564 may also have high spins, with values of $a = 0.79(1)$ and $a = 0.76(1)$, respectively. In each of these four cases, relatively high spin values might have been anticipated based on prior suggestions, whether from various interpretations of high-frequency QPOs, previous fits to the Fe K line shape, or extreme jet phenomena. It should be noted that the implied inclination of GX 339–4 does not imply a very high black hole mass based on the work of Hynes et al. (2003), as the inclination of the inner disk and binary system need not be the same (see Maccarone 2002).

The spin obtained for XTE J1908+094 is nominally rather high as well, at $a = 0.75(9)$. The value obtained for SAX J1711.6–3808 is more moderate, at $a = 0.6(2)$. These two values are discussed in more detail below.

Within our sample, Cygnus X-1 stands out as the only high-mass X-ray binary. The observations of Cygnus X-1 considered in this work were made in a "high" state, where the Fe K line is known to be stronger, perhaps broader (Cui et al. 1998), and perhaps more suggestive of emission from the ISCO (Gilfanov, Churazov, & Revnivtsev 2000) than in the "low/hard" state. At $a = 0.05(1)$, Cygnus X-1 is ostensibly found to harbor a black hole with very low spin. It is interesting to note that fits to the black hole with the next highest companion mass, 4U 1543–475, also give a low spin parameter of 0.3(1).

To better understand possible physical connections, Figures 18–20 plot the spin values that we have obtained versus black hole mass, versus the ratio of black hole mass to companion mass, and versus orbital period using the parameters in Table 1 and Table 2. There is no clear evidence that spin is correlated with any of these parameters. The most promising case for a correlation is between the black hole spin parameter and binary mass ratio (see Figure 19). However, more sources and improved errors on the ratio values needed to make any relation significant.

3.3. *On the Robustness of the Spin Constraints*

When fitting a complex model in packages such as XSPEC or ISIS, special care is needed. Convolution models, table models, and total models with many individual components are especially prone to saddle points in χ^2 space. In these cases, efforts to minimize χ^2 are improved with a hands-on approach. In our analysis, fits were made within XSPEC in the usual way – until the minimum required change in χ^2 had nominally been met. Then, we pushed random parameters off of their best-fit values by factors of 10–30%, and re-fit the data. This procedure was repeated many times in an effort to make sure that a *global* minimum was found. Then, we calculated 1σ errors on the parameters in the model using the "error" command, which calculates a joint error in that it allows other parameters to float.

Although this fitting procedure likely improved the rigor of our results, the errors quoted in Table 2 and Table 3 do not fully convey the nature of some spin values. In some cases, the χ^2 space is complex, and though there is a nominal preference for a particular spin value, extremal values may not excluded at high significance. We examined this possibility using the "steppar" command within XSPEC. This command affords greater control over how the χ^2 space is searched. For each source, the spin parameter was frozen at twenty evenly-spaced values between zero and unity while all other parameters were allowed to vary. We checked the results of steppar by manually executing the same procedure. The manual procedure gave more conser-

vative results than steppar for GRO J1655–40; the conservative results are plotted in Figure 21. Figures 21–23 plot the dependence of χ^2 on the black hole spin parameter a, for each black hole in our sample.

The spin parameters measured for XTE J1550–564 and GX 339–4 exclude $a = 0$ at far more than the 8σ level of confidence; for GRO J1655–40 and XTE J1650–500, zero spin is excluded at the 6σ level of confidence (see Figure 21). The results from Cygnus X-1 strongly suggest a low spin value, and we performed a similar check on that result. High spin values (e.g. $a > 0.9$) for Cygnus X-1 at more than the 8σ level of confidence (see Figure 22). However, other spin constraints are less certain. For 4U 1543–475, $a = 0$ is only excluded at the 3σ level of confidence, although high spin is excluded at more than the 8σ level of confidence. The spins parameters reported for SAX J1711.6–3808 and XTE J1908+094 are not confidently determined (see Figure 23). Zero spin is just outside of the 1σ range for SAX J1711.6–3808, and a maximal spin value is only excluded at the 2σ level of confidence. Similarly, fits to XTE J1908+094 only exclude minimal and maximal spin at the 2σ level of confidence.

The most important source of systematic error in our results may derive from theoretical uncertainties in the "effective" ISCO. We have assumed that the inner radius of the disk is the ISCO as defined by test particle orbits. In an actual fluid disk, the effective inner disk radius may differ slightly from the nominal ISCO. The most recent and sophisticated simulations that address this issue are summarized in Reynolds & Fabian (2008); that work is especially relevant because the disk is taken to be *thin*. (Prior simulations considered hot, thick disks, which are unlikely to apply in the regimes sampled by our data; see, e.g., Krolik, Hawley, & Hirose 2005.) The surface density and ionization parameter of orbiting gas is found to change sharply at the ISCO. Based on the results summarized in Reynolds & Fabian (2008) and related work by Shafee et al. (2008), a conservative estimate of the uncertainty in the ISCO based on this and other simulations is $0.5\ r_g$ for low spin parameters (an uncertainty of about 20% for very low spin; see Miniutti & Fabian 2009); the uncertainty is less for high spin parameters.

Prior work on GX 339–4 is helpful in estimating systematic errors related to the state in which a source is observed. Miller et al. (2008) find that the spin parameter derived from fits to a single spectrum from a given state differ from those derived by jointly multiple spectra from three states by only 4%. Prior work on this source is also helpful in evaluating systematic effects due to different disk reflection models. Reis et al. (2008) fit spectra of GX 339–4 with a new disk reflection model, in which the atmosphere is directly influenced by blackbody emission in the midplane. Despite the different reflection models employed by Miller et al. (2008) and Reis et al. (2008), the spin parameters derived are fully consistent. At least in the case of stellar-mass black holes with high inferred spin parameters, then, modest differences in disk reflection models do not strongly affect spin results.

Detector calibration is another potential source of systematic error. In the case of disk reflection features, however, the degree of systematic error is likely to be small. Silicon-based detectors often suffer a sharp change in effective area around 2 keV, but these features can be modeled and should not strongly affect the 4–8 keV range. Calibration uncertainties also typically arise below 0.7 keV in CCD spectra; here again, uncertainties in this region will not affect fits at much higher energy. The response of xenon-based gas detectors may be a larger source of systematic error: the Xe L3 edge at 4.78 keV – if not modeled correctly – can affect fits to relativistic iron lines.

Most of the strong constraints that we have obtained come from CCD spectra; the results obtained from XTE J1550–564 are the exception. This suggests that the resolution afforded by CCD spectrometers plays an important role in obtaining black hole spin constraints. The energy resolution of most gas spectometers is $E/dE \sim 6$. At 6 keV, that is a resolution of 1 keV, or about $0.17c$ – a large fraction of the velocity of matter orbiting at the ISCO. Only extremely strong emission lines will permit strong constraints in data obtained with gas spectrometers.

3.4. *On the Role of the Disk Continuum*

Fits obtained with the simple "diskbb" disk continuum model (Mitsuda et al. 2004) are, in general, statistically comparable to fits made using the "kerrbb" model (Li et al. 2005) and yield similar spin parameters, though in this case the spin is only measured through the relativistic reflection signatures (see Table 2 and Table 3). A notable exception may be 4U 1543–475: stronger spin constraints are derived when the "kerrbb" model is used. We have assumed that the inclination of the inner disk in 4U 1543–475 equals the binary inclination, which is tightly constrained (Park et al. 2004). The fact that "kerrbb" includes the inclination as a free parameter – which is coupled to the inclination in the blurred reflection model – may account for the improvement.

The dominant role of the disk reflection spectrum is consistent with some simple expectations. Whereas a disk line bears the imprints of gravitational red-shifts and Doppler shifts, disk continua do not manifest equally unambiguous signatures of black hole spin. An especially high temperature – perhaps indicative of a high efficiency and black hole spin – can instead be explained by a high mass accretion rate. Similarly, a small emitting area can potentially be explained in terms of incorrectly accounting for scattering of the thermal continuum in the disk.

Systematic uncertainties in necessary physical inputs may also have kept the disk continuum from driving most of the spin values. Most of the uncertainties in black hole mass and distance listed in Table 1 are rather large, in a fractional sense. Moreover, different cameras aboard the same observatory do not necessarily measure the same flux level. In our fits to the two *ASCA*/GIS spectra of XTE J1550–564, for instance, we have handled such systematics by allowing the cameras to find different thermal disk properties apart from the black hole spin parameter (values generally differ by less than 20%). The procedure we have adopted is a compromise between the principle of using physical models and the need to acknowledge real observational limitations.

Although the simpler disk continuum model generally produced equivalent results, we regard the results obtained using the more physical continuum models as more definitive for three reasons. First, the physical models do not give fits that are dramatically inferior, in a statistical sense. Second, the physical models do not appear to skew the spin parameters in a particular direction. Finally, and perhaps most importantly, the physical disk models do attempt to account for important processes and spin explicitly, and so enable a degree of self-consistency in the total spectral model.

4. DISCUSSION

We have analyzed X-ray spectra from eight stellar-mass black holes. The spectra were modeled with a combination of a relativistically-blurred disk reflection spectrum and a new disk continuum model in which spin is a variable parameter. Spin estimates were jointly derived by linking the spin parameters in the reflection and continuum models. This is the first effort to estimate spin parameters in a number of sources by combining these independent spectral diagnostics. Our results suggest that stellar-mass black holes may have a range of spin parameters. Below, we discuss the implications of this finding for black hole creation events, relativistic jet production, and efforts to probe the innermost relativistic regime around black holes.

A black hole needs to accrete a large fraction of its mass to reach maximal spin (Volonteri et al. 2005). In the case of stellar-mass black holes, then, spin parameters should be determined primarily by the supernova or gamma-ray burst event that creates the black hole. Theoretical investigations into nascent black hole spin parameters, set by a single collapse event, have focused on supermassive stars in the early universe. Only considering the collapse event, a spin of $a \simeq 0.75$ is expected (Shibata & Shapiro 2002); with additional considerations, a spin as high as $a \leq 0.93$ may be possible (Gammie et al. 2004). Our results are nominally at odds with these predictions. However, as noted by Heger & Woosley (2002) and Gammie et al. (2004), the mass, angular momentum, metallicity, and magnetic field structure in progenitor stars are all important in determining its final spin, and considerable theoretical uncertainties remain in modeling this problem. More theoretical and observational work is needed before it is clear that collapse/explosion models are incorrect or that some black holes were formed in exotic circumstances.

The most extreme result we have obtained may be the near-zero spin for Cygnus X-1. The *XMM-Newton* spectra that we analyzed were obtained in a "high" state (called the "very high" state in other black holes); this makes it very unlikely that the disk was far from the ISCO when the source was observed. Additional observational work with *Suzaku* is needed to confirm a low spin parameter. The fact that some SNe leave behind neutron stars with modest magnetic fields, while others give rise to magnetars, is one important indication that stellar explosions can leave behind objects with very different properties. Cygnus X-1 is the only high-mass binary in our sample, and this property may be important in determining its spin. Indeed, Cygnus X-1 may be even more special: Mirabel & Rodrigues (2003) suggest that Cygnus X-1 may have formed in an unusual supernova with very little mass loss, owing to the absence of a supernova remnant and its low space velocity.

A connection between spin and jets is anticipated theoretically (e.g. Blandford & Znajek 1977), and our results would appear to hint at a connection: GX 339–4, GRO J1655–40, and XTE J1550–564 are all relativistic jet sources where velocities above $0.9c$ have been inferred (Gallo et al. 2004, Hjellming & Rupen 1995, Hannikainen et al. 2001), and all of them are found to have relatively high spin values. A high spin parameter is also implied in XTE J1650–500, but no relativistic jet was detected in this source. The absence of such a detection may be due to the limited angular resolution of instruments in the Southern Hemisphere. Cygnus X-1 may again be an important exception: our fits imply a very low spin parameter, yet Cygnus X-1 powers a jet with $v/c \geq 0.6$ (Stirling et al. 2001).

Taken as a whole, our results only weakly support a link between spin and jet power. Future observations of black hole transients in both X-ray and radio bands may be able to build a sample from which stronger conclusions can be drawn. Not every black hole in our sample was observed intensively in the radio band or at high angular resolution; relativistic jets could have been missed in some sources. Moreover, spin may not be the only parameter important in producing relativistic jets, especially since jets are not seen in all black hole states. Garcia et al. (2003) found that relativistic jet sources tend to be those with long orbital periods. It might be the case that a parameter such as the absolute mass accretion rate through the disk is important.

It is worth noting that in the cases where high spin parameters are required by our spectral models, the line emissivity index is found to be very steep ($q \sim 5$). Both a high spin parameter and a steep emissivity index would serve to concentrate the reflected emission in the very innermost part of the disk. High spin parameters are therefore required despite steep emissivity profiles, not because of steep emissivity profiles. Physically, an emissivity of $q > 3$ may imply that the source of hard X-ray flux in these systems may be very compact, and may radiate anisotropically. Prior work has suggested that the compact coronae implied may be consistent with the base of a jet (e.g. Miller et al. 2004b). This inner accretion flow geometry is similar to that described in models for line and continuum variability that invoke gravitational light bending close to a spinning black hole (see Miniutti & Fabian 2004). Gravitational light-bending may be partially responsible for concentrating emission centrally. Investigations of line variability in Seyfert AGN with the *International X-ray Observatory* (IXO) will be able to provide much stronger evidence of gravitational light bending.

The new results reported in this work are broadly consistent with prior estimates of black hole spin using line models with fixed spin parameters. For instance, in the case of XTE J1650–500, prior fits to spectra obtained with *XMM-Newton* and *BeppoSAX* indicated inner disk radii of $2r_g$ or less (Miller et al. 2002; Miniutti, Fabian, & Miller 2004). Prior fits to *Chandra* and *XMM-Newton* spectra of GX 339–4 strongly suggested a high spin parameter (Miller et al. 2004a, 2004b, 2006); later fits to *XMM-Newton* and *Suzaku* spectra with variable-spin disk reflection models yielded results consistent with those reported here (Miller et al. 2008; see also Reis et al. 2008).

The spin parameters that we have obtained for 4U 1543–475 and GRO J1655–40 do not fully agree with recent modeling of the accretion disk continuum alone (Shafee et al. 2006; also see Zhang, Cui, & Chen 1997). Whereas we measure $a = 0.3(1)$ for 4U 1543–475, Shafee et al. (2006) find $a = 0.75 - 0.85$. And whereas we measure $a = 0.98(1)$ for GRO J1655–40, Shafee et al. (2006) give $a = 0.65 - 0.75$. The differences may be partially derive from lingering systematic errors and differing analysis procedures. As noted previously, spin estimates based on the continuum require an absolute flux measurement, and so require accurate knowledge of the mass and distance to the source, and incur systematics due to uncertainties in the absolute flux calibration of a given instrument. In a number of fits, Shafee et al. (2006) only consider *RXTE* spectra below 8 keV, and in other cases the line and reflection continuum is modeled with a Gaussian and (unphysical) smeared edge. The disk reflection spectrum, which is less subject to systematic uncertainties, appears to drive the spin constraints we have obtained. In the broadest sense, future work aimed at resolving the differences such as $a = 0.3(1)$ versus a =0.75-0.85 (for 4U 1543–475) and $a = 0.98(1)$ versus a =0.65-0.75 (for GRO J1655–40) is

a welcome prospect and marks a turning point for studies of stellar-mass black holes.

The results we have obtained underscore the urgent need to obtain X-ray spectra of multiple sources in multiple states, with moderate or high resolution spectrometers. Observing multiple states and jointly fitting resultant spectra to require a common spin parameter (Miller et al. 2008, Reis et al. 2008) ensures that any variations in the ionization and/or structure of the accretion disk are treated explicitly. *Chandra* and *XMM-Newton* are both well-suited to this aim; the broad-band spectroscopy and high throughput, fast CCD read-out of *Suzaku* mean it is an exceptional tool for disk reflection studies. Future missions, including *Astro-H* (NeXT) and the *IXO* will be able to measure spin in stellar-mass black holes with unprecedented precision, if high source fluxes can be accommodated. The knowledge gained in understanding the spin distribution of stellar-mass black holes can be transferred to studies of supermassive black hole spins.

Our results also highlight the need to measure more black hole masses through dynamics, and to push current and future mass constraints to higher precision. Even in this initial attempt at a systematic analysis, it is already clear that uncertainties in binary parameters inhibit stronger conclusions. If we are to understand how supernovae and GRBs might produce black holes with differing spin parameters, robust measurements of the remnant black hole mass, its companion mass, and other system parameters will be important factors. Especially when a black hole lies in a region with high line-of-sight column density, rapid IR observations may help to identify counterparts and enable later dynamical studies. The properties of GRS 1915+105 have not yet been measured precisely (Greiner, Cuby, & McCaughrean et al. 2001), but the fact that measurements are possible given a acolumn density of $N_H \simeq 4 \times 10^{22}$ atoms cm^{-2} (Dickey & Lockman 1990) signals that there is a way forward in such cases.

5. CONCLUSIONS

We have fitted relativistic disk reflection and disk continuum models to a number of stellar-mass black holes. A broad range of spin parameters is measured. This implies a fundamental diversity in the GRB/SNe events that are thought to create stellar-mass black holes. The black holes with the highest spin parameters are those wherein the most relativistic jets have been observed in radio bands, providing modest support for a connection between spin and jets. With a larger sample, the influence of binary system parameters (if any) on black hole spin may become apparent.

We acknowledge the anonymous referee for comments that improved this manuscript.We wish to thank Jean in 't Zand for generously making the *BeppoSAX* spectra of SAX J1711.6−3808 and XTE J1908+094 available. We acknowledge helpful conversations with Charles Gammie, Julian Krolik, and Cole Miller. J. M. M. thanks Keith Arnaud, Brian Irby, and Roy Bonser for help with XSPEC and HEASOFT. C. S. R. acknowledges support from the NSF under grant AST06-07428. G. M. thanks the Spanish Ministerio de Ciencia e Innovación and the CSIC for support through a Ramón y Cajal contract. This work made use of the tools and information available through the HEASARC facility, operated for NASA by GSFC.

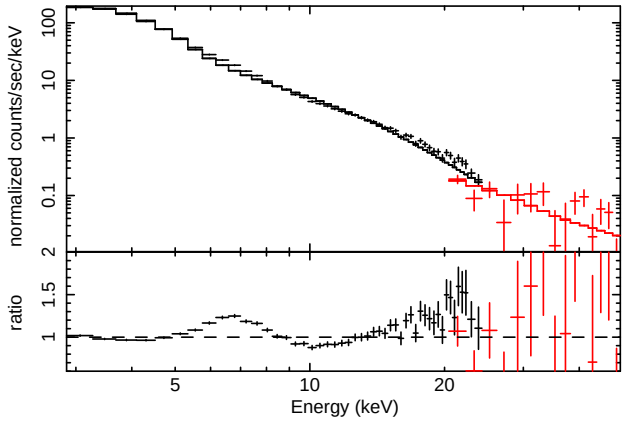

FIG. 1.— The plot above shows the *RXTE* spectrum of 4U 1543–475 fit with a phenomenological disk plus power-law model. The 4–7 keV range was ignored when fitting the spectrum to best illustrate the relativistic iron line.

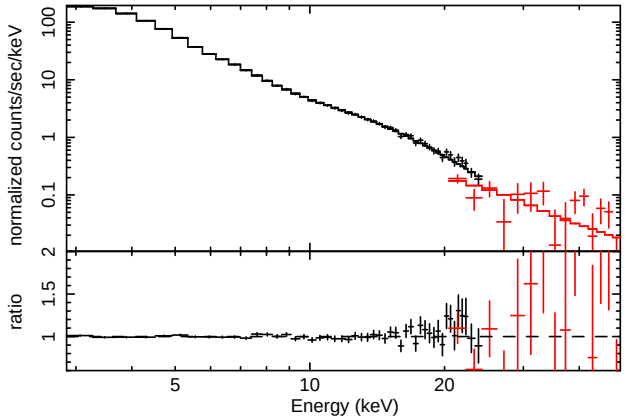

FIG. 2.— The plot above shows the *RXTE* spectrum of 4U 1543–475 fit with a relativistically-blurred reflection spectrum and the "kerrbb" disk continuum model. The spin parameters in the disk reflection and continuum spectra were linked.

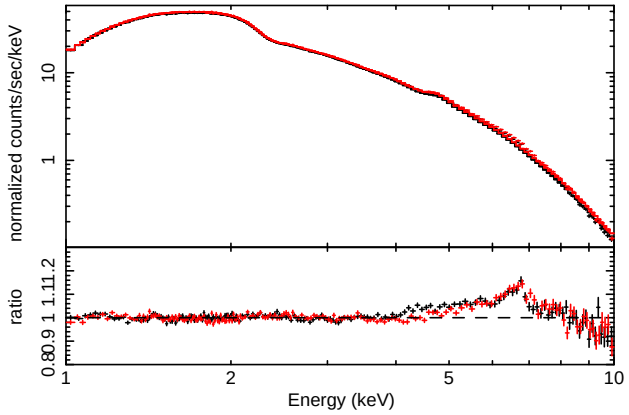

FIG. 3.— The plot above shows the *ASCA* spectra of XTE J1550–564 fit with a phenomenological disk plus power-law model. The 4–7 keV range was ignored when fitting the spectra to best illustrate the relativistic iron lines.

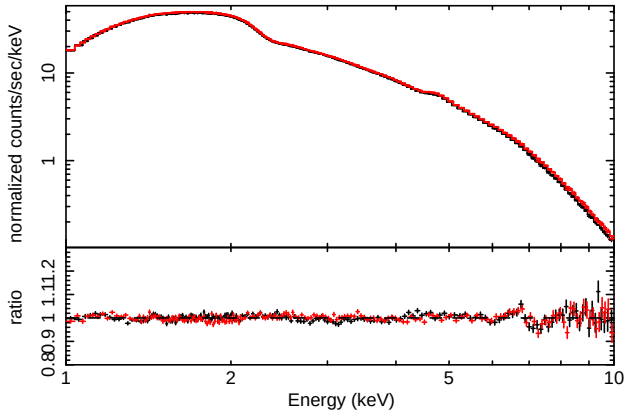

FIG. 4.— The plot above shows the *ASCA* spectra of XTE J1550–564 fit with a relativistically-blurred reflection spectrum and the "kerrbb" disk continuum model. The spin parameters in the disk reflection and continuum spectra were linked.

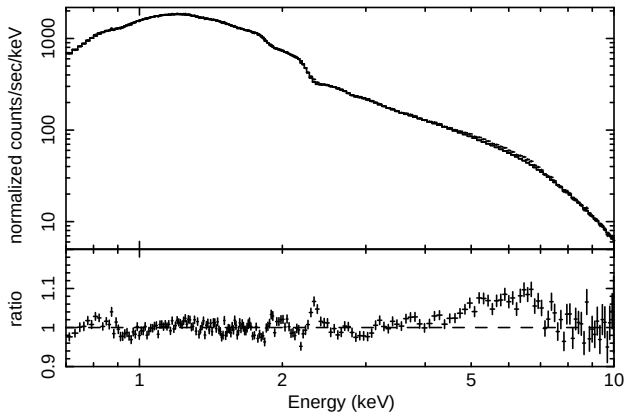

FIG. 5.— The plot above shows the *XMM-Newton* spectrum of XTE J1650–500 fit with a phenomenological disk plus power-law model. The 4–7 keV range was ignored when fitting the spectrum to best illustrate the relativistic iron line. Features around 2 keV are instrumental.

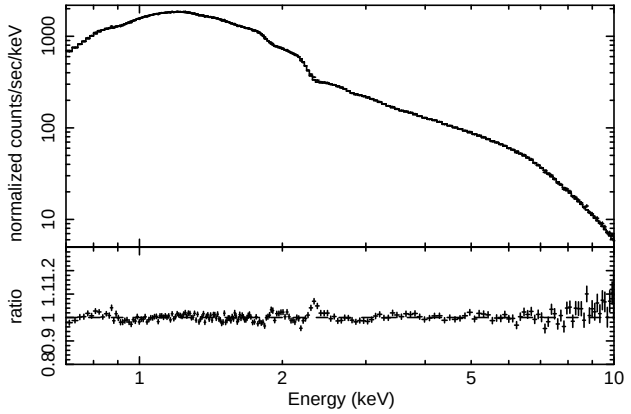

FIG. 6.— The plot above shows the *XMM-Newton* spectrum of XTE J1650–500 fit with a relativistically-blurred reflection spectrum and the "kerrbb" disk continuum model. The spin parameters in the disk reflection and continuum spectra were linked.

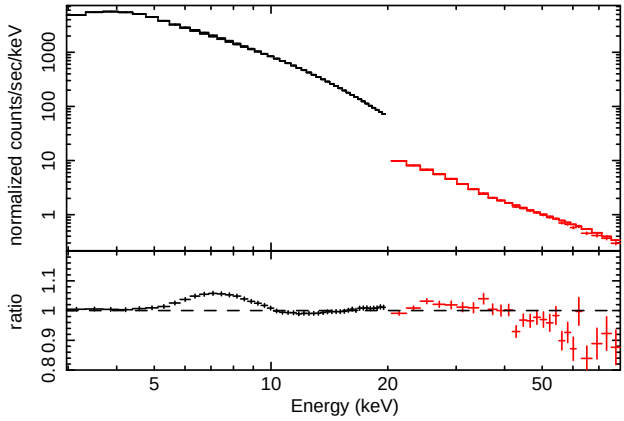

FIG. 7.— The plot above shows the *RXTE* spectra of GRO J1655–40 fit with a phenomenological disk plus power-law model. The 4–7 keV range was ignored when fitting the spectrum to best illustrate the relativistic iron line.

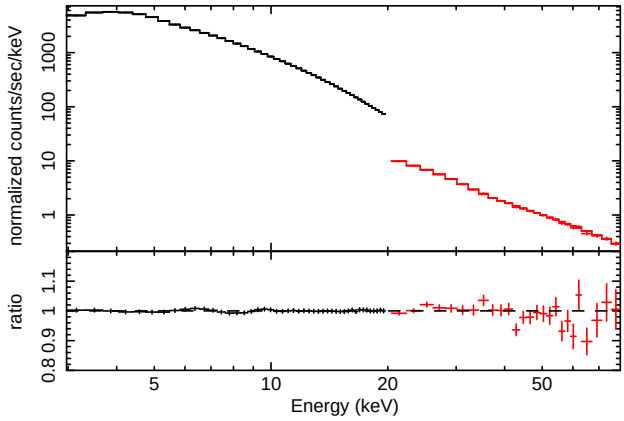

FIG. 8.— The plot above shows the *RXTE* spectra of GRO J1655–40 fit with a relativistically-blurred reflection spectrum and the "kerrbb" disk continuum model. The spin parameters in the disk reflection and continuum spectra were linked.

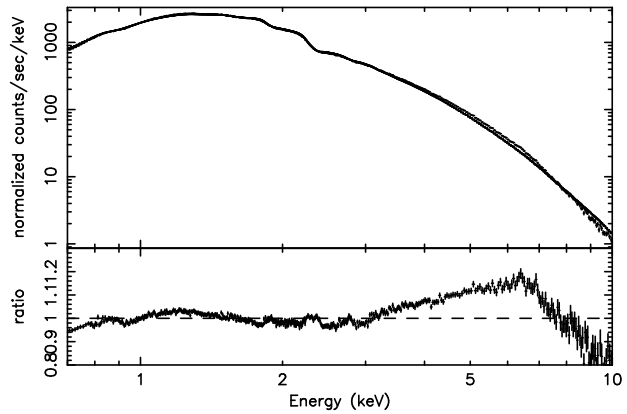

FIG. 9.— The plot above shows the *XMM-Newton* spectrum of GX 339–4 fit with a phenomenological disk plus power-law model. The 4–7 keV range was ignored when fitting the spectrum to best illustrate the relativistic iron line. Features around 2 keV are instrumental.

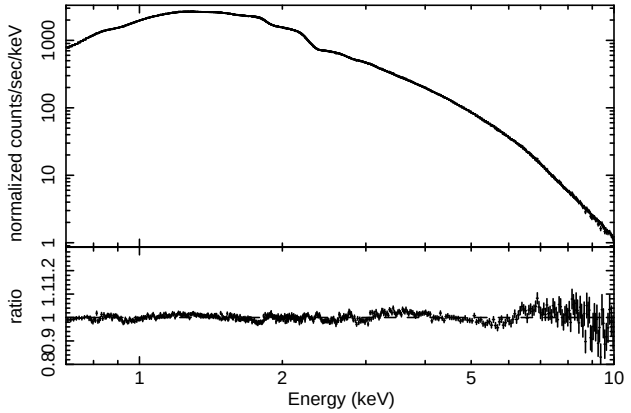

FIG. 10.— The plot above shows the *XMM-Newton* spectrum of GX 339–4 fit with a relativistically-blurred reflection spectrum and the "kerrbb" disk continuum model. The spin parameters in the disk reflection and continuum spectra were linked.

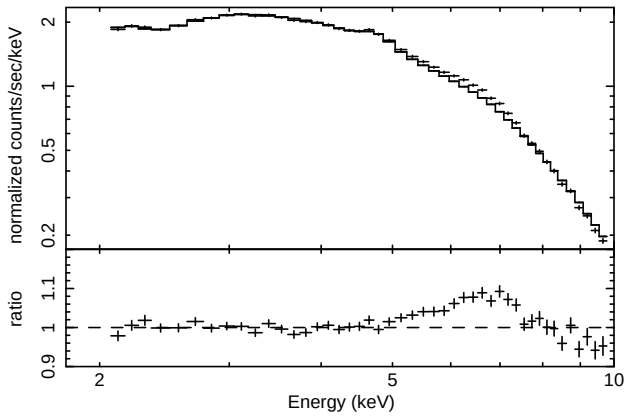

FIG. 11.— The plot above shows the *BeppoSAX* spectrum of SAX J1711.6–3808 fit with a phenomenological power-law model. The 4–7 keV range was ignored when fitting the spectrum to best illustrate the relativistic iron line.

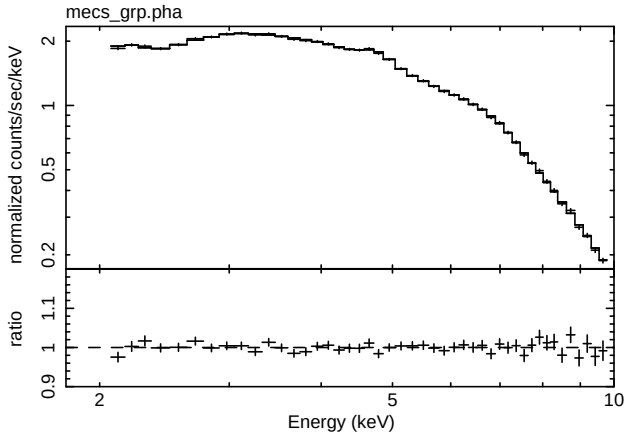

FIG. 12.— The plot above shows the *BeppoSAX* spectrum of SAX J1711.6–3808 fit with a relativistically-blurred reflection model.

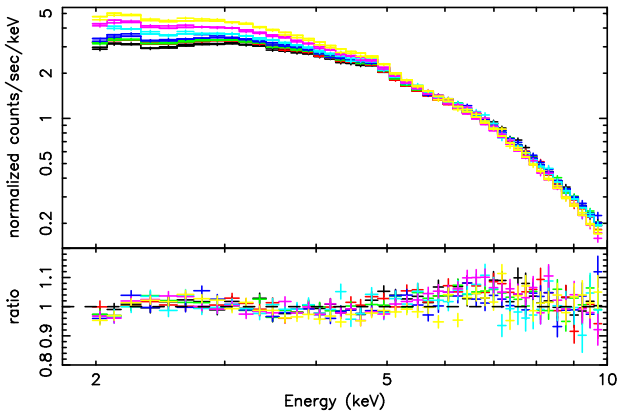

FIG. 13.— The plot above shows the *BeppoSAX* spectra of XTE J1908+094 fit with a phenomenological power-law model. The 4–7 keV range was ignored when fitting the spectrum to best illustrate the relativistic iron line.

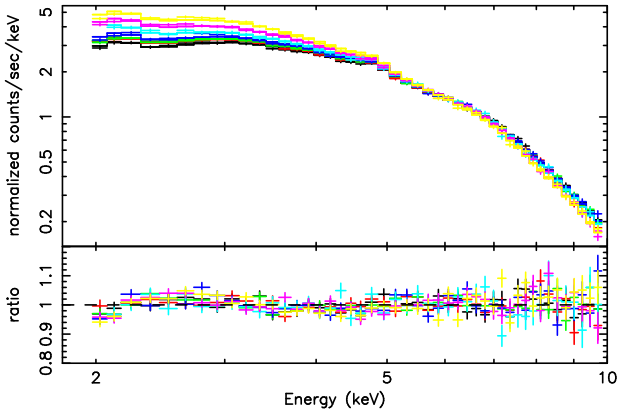

FIG. 14.— The plot above shows the *BeppoSAX* spectra of XTE J1908+094 fit with a relativistically-blurred reflection model.

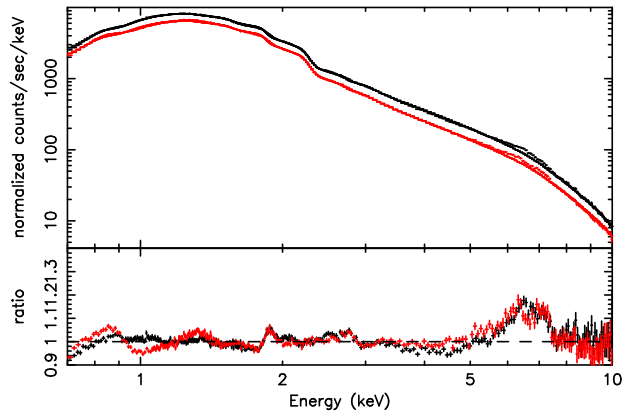

FIG. 15.— The plot above shows the *XMM-Newton* spectra of Cygnus X-1 fit with phenomenological disk plus power-law models. The 4–7 keV range was ignored when fitting the spectra to best illustrate the relativistic iron lines. Features around 2 keV are instrumental.

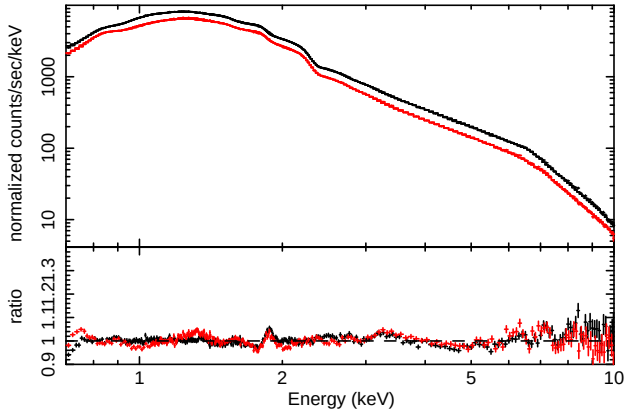

FIG. 16.— The plot above shows the *XMM-Newton* spectra of Cygnus X-1 fit with a relativistically-blurred reflection spectrum and the "kerrbb" disk continuum model. The spin parameters in the disk reflection and continuum spectra were linked.

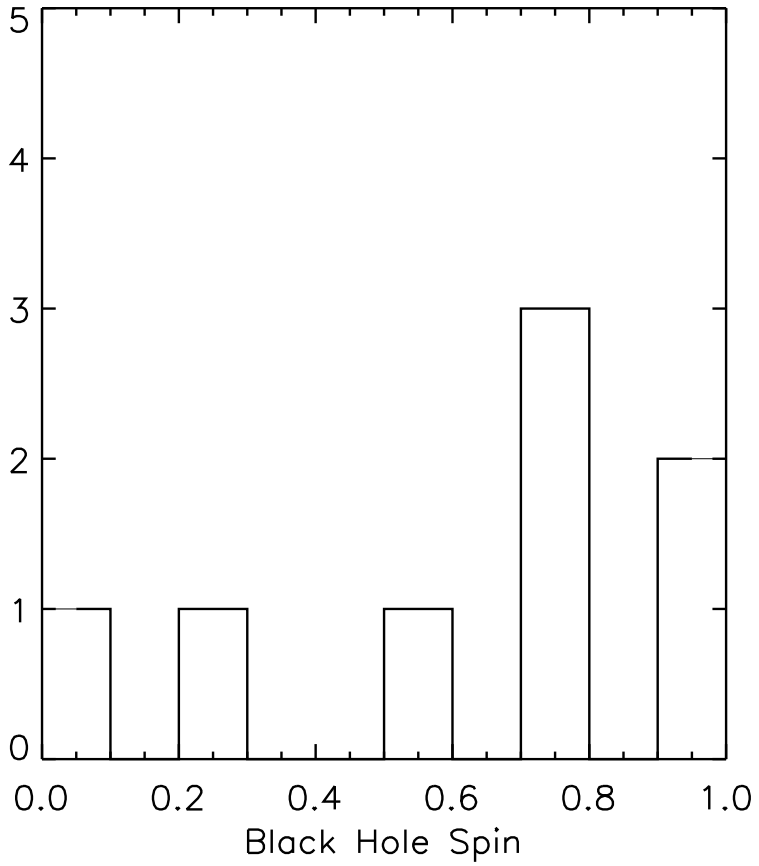

FIG. 17.— The histogram above plots the distribution of black hole spin parameters obtained through our fits. Please see the text for details and caveats.

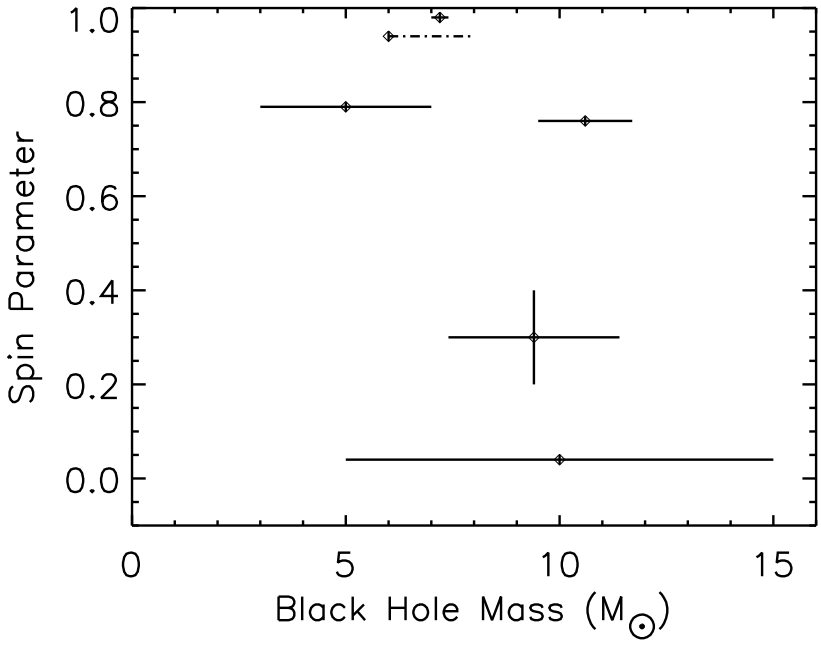

FIG. 18.— The plot above shows our derived 1σ spin constraints versus black hole mass, for sources with known masses. The dashed, single-sided error above denotes that only a lower mass limit has been obtained for GX 339–4. Please see Section 2 for more details.

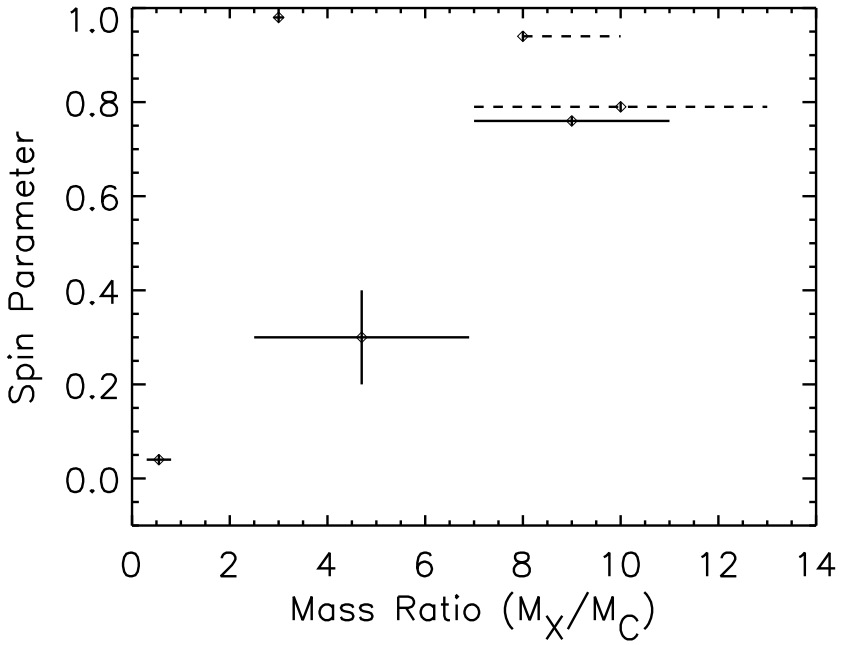

FIG. 19.— The plot above shows our derived 1σ spin constraints versus the ratio of the black hole mass to the companion mass, for sources with known masses. The dashed, single-sided error above denotes that only a lower limit has been obtained for the mass ratio in GX 339–4. The dashed, double-sided error denotes that the mass ratio in XTE J1650–500 is largely unconstrained.

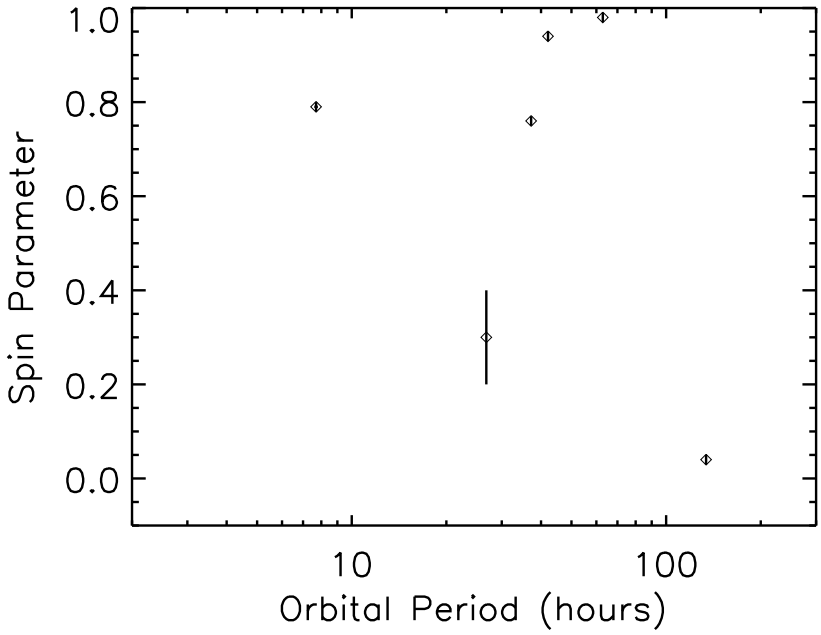

FIG. 20.— The plot above shows our derived 1σ spin constraints versus the orbital period of the binary, for sources with known masses. The errors on orbital period are plotted but they are very small.

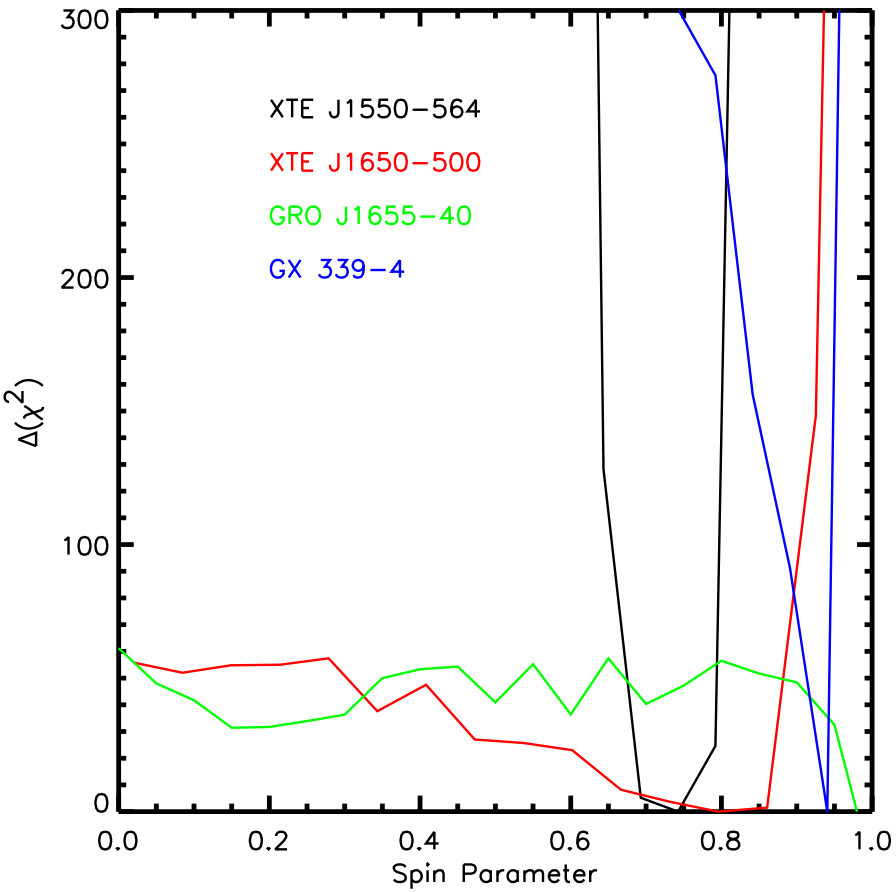

FIG. 21.— The plot above shows the change in the goodness-of-fit statistic as a function of the black hole spin parameter, *a*. Using the XSPEC "steppar" command, 20 evenly-spaced value of *a* were frozen and all other parameters were allowed to float freely to find the best fit at that spin parameter. For clarity, only sources measured to have high spin at high confidence are shown above.

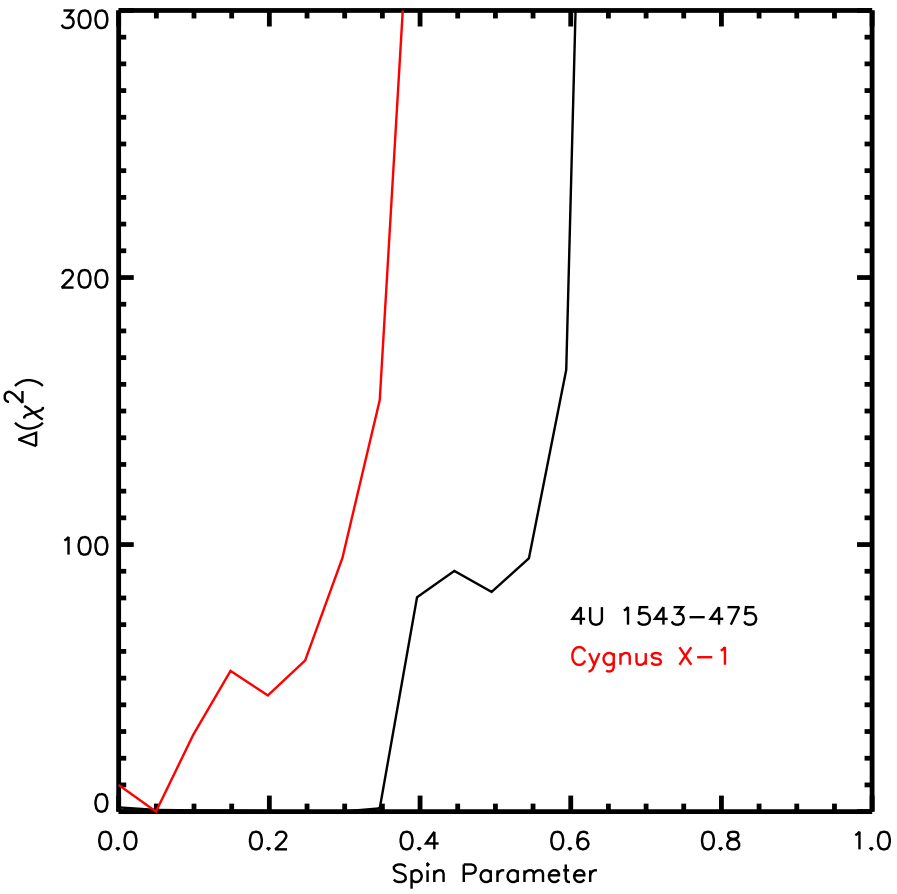

FIG. 22.— The plot above shows the change in the goodness-of-fit statistic as a function of the black hole spin parameter, *a*. Using the XSPEC "steppar" command, 20 evenly-spaced value of *a* were frozen and all other parameters were allowed to float freely to find the best fit at that spin parameter. For clarity, only sources measured to low high spin at high confidence are shown above.

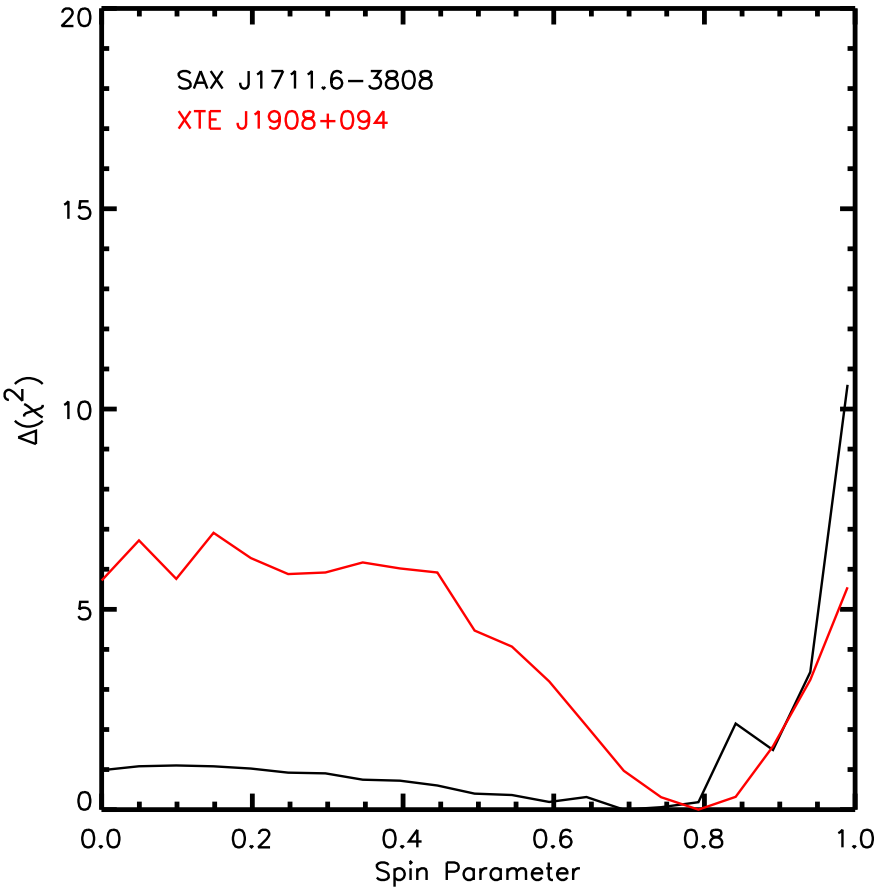

FIG. 23.— The plot above shows the change in the goodness-of-fit statistic as a function of the black hole spin parameter, *a*. Using the XSPEC "steppar" command, 20 evenly-spaced value of *a* were frozen and all other parameters were allowed to float freely to find the best fit at that spin parameter. For clarity, only sources for which spin is not confidently determined are shown above.

REFERENCES

Arnaud, K. A., and Dorman, B., 2000, XSPEC is available via the HEASARC on-line service, provided by NASA/GSFC
Ballantyne, D., Ross, R. R., & Fabian, A. C., 2001, MNRAS, 327, 10
Balucinska-Church, M., & Church, M. J., 2000, MNRAS, 311, 861
Beckwith, K., & Done, C., 2004, MNRAS, 352, 353
Blandford, R. D., & Znajek, R. L., 1977, MNRAS, 179, 433
Blum, J. L., et al., 2009, ApJ, in preparation
Brandt, W. N., et al., 1996, MNRAS, 283, 1071
Brenneman, L. W., & Reynolds, C. S., 2006, ApJ, 652, 1028
Bhattacharyya, S., & Strohmayer, T. E., 2007, ApJ, 664, L103
Cackett, E., et al., 2008, ApJ, 674, 415
Chartas, G., Kochanek, C. S., Dai, X., Poindexter, S., & Garmire, G., 2008, ApJ, in press
Cui, W., Ebisawa, K., Dotani, T., & Kubota, A., 1998, ApJ, 493, L75
Diaz Trgo, M., Parmar, A. N., Miller, J. M., Kuulkers, E., Caballero-Garcia, M. D., et al., 2007, A&A, 462, 657
Dickey, J. M., & Lockman, F. J., 1990, ARA&A, 28, 215
Dovciak, M., Karas, V., & Yaqoob, T., 2004, ApJS, 153, 205
Frank, J., King, A., & Raine, D., 2002, in "Accretion Power in Astrophyiscs", Cambridge University Press, Cambridge
Gallo, E., Corbel, S., Fender, R. P., Maccarone, T. J., & Tzioumis, A. K., 2004, MNRAS, 347, L52
Gallo, E., et al., 2009, in preparation
Gammie, C. F., Shapiro, S. L., & McKinney, J. C., 2004, ApJ, 602, 312
Garcia, M. R., Miller, J. M., McClintock, J. E., King, A. R., & Orosz, J., 2003, ApJ, 591, 388
Gilfanov, M., Churazov, E., & Revnivtsev, M., 2000, MNRAS, 316, 923
Greiner, J., Cuby, J. G., & McCaughrean, M. J., 2001, Nature, 414, 522
Hannikainen, D., et al., 2001, ApSSS, 276, 45
Heger, A., & Woosley, S., 2002, ApJ, 567, 532
Herrero, A., et al., 1995, A&A, 297, 556
Hjellming, R. M., & Rupen, M. P., 1995, Nature, 375, 464
Homan, J., et al., 2001, ApJS, 132, 377
Hynes, R. I., Steeghs, D., Casares, J., Charles, P. A., & O'Brien, K., 2003, ApJ, 583, L95
Hynes, R. I., Charles, P. A., van Zyl, L., Barnes, A., Steeghs, D., O'Brien, K., & Casares, J., 2004, MNRAS, 348, 100
van der Klis, M., 2001, ApJ, 561, 943
van der Klis, M., 2006, in "Compact Stellar X-ray Sources", eds. W. Lewin and M. van der Klis, Cambridge University Press: Cambridge
Krolik, J. H., Hawley, J., & Hirose, S., 2005, ApJ, 622, 1008
Laor, A., 1991, ApJ, 376, L90
Li, L., Zimmerman, E. R., Narayan, R., McClintock, J. E., 2005, ApJS, 157, 335
Maccarone, T., 2002, MNRAS, 336, 1371
Martin, R. G., Reis, R. C., & Pringle, J. E., 2008, MNRAS, in press
Martocchia, A., Matt, G., Karas, V., Belloni, T., & Feroci, M., 2002, A&A, 387, 215
McClintock, J. E., et al., 2006, ApJ, 652, 518
Miller, J. M., et al., 2002, ApJ, 570, L69
Miller, J. M., et al., 2002b, ApJ, 577, L15
Miller, J. M., et al., 2004a, ApJ, 606, L131
Miller, J. M., Fabian, A. C., Nowak, M. A., & Lewin, W. H. G. L., 2005, in the proceedings of the Tenth Marcel Grossmann Meeting, eds. M. Novello, S. Perez Berliaffa, R. Ruffini, Singapore: World Scientific
Miller, J. M., Homan, J., Steeghs, D., Rupen, M., Hunstead, R. W., Wijnands, R., Charles, P., & Fabian, A. C., 2006, ApJ, 653, 525
Miller, J. M., et al., 2006, ApJ, 653, 525
Miller, J. M., et al., 2006b, Nature, 441, 953
Miller, J. M., 2007, ARA&A, 45, 441
Miller, J. M., et al., 2008, ApJ, 679, L113
Miller, J. M., et al., 2008b, ApJ, 680, 1359
Miniutti, G., Fabian, A. C., & Miller, J. M., 2004, MNRAS, 351, 466
Miniutti, G., & Fabian, A. C., 2004, MNRAS, 349, 1435
Miniutti, G., & Fabian, A. C., 2009, to appear in "Kerr Spacetime: Rotating Black Holes in General Relativity", eds. D. L. Wiltshire, M. Visser, & S. M. Scott, Cambridge University Press, Cambridge
Miniutti, G., et al., 2007, PASJ, 59, 315
Mirabel, F., & Rodrigues, I., 2003, Science, 300, 1119
Mitsuda, K., et al., 1984, PASJ, 36, 741
Munoz-Darias, T., Casares, J., & Martinez-Pais, I. G., 2008, MNRAS, 385, 2205
Orosz, J., & Bailyn, C. D., 1997, ApJ, 477, 876
Orosz, J., et al., 2002, ApJ, 568, 845
Orosz, J., et al., 2004, ApJ, 616 376
Park, S. Q., et al., 2004, ApJ, 610, 378
Reis, R. C., Fabian, A. C., Miniutti, G., Miller, J. M., & Reynolds, C., 2008, MNRAS, 387, 1489
Remillard, R. A., & McClintock, J. E., 2006, ARA&A, 44, 49
Revnivtsev, M., Sunyaev, R., Gilfanov, M., & Churazov, E., 2002, A&A, 385, 904
Reynolds, C. S., & Fabian, A. C., 2008, ApJ, in press, arxiv:0711.4158
Reynolds, C. S., & Miller, M. C., 2008, ApJ, subm., arxiv:0805.2950
Ross, R. R., & Fabian, A. C., 2007, MNRAS, 381, 1697
Rossi, S., Homan, J., Miller, J. M., & Belloni, T., 2005, MNRAS, 360, 763
Rykoff, E. S., Miller, J. M., Steeghs, D., & Torres, M. A. P., 2007, ApJ, 666, 1129
Shafee, R., et al., 2006, ApJ, 636, L113
Shafee, R., et al., 2008, ApJ, subm.
Shibata, M., & Shapiro, S. L., 2002, ApJ, 572, L39
Sikora, M., Stawarz, L., & Lasota, J. P., 2007, ApJ, 658, 815
Sobczak, G. J., et al., 1999, ApJ, 520, 776
Stirling, A. M., et al., 2001, MNRAS, 327, 1273
Swank, J., Smith, E. A., Smith, D. M., & Markwardt, C. B., 2006, ATEL 944
Takahashi, H., et al., 2008, PASJ, 60, 69
Volonteri, M., Madau, P., Quataert, E., & Rees, M. J., 2005, ApJ, 620, 69
Wijnands, R., & Miller, J. M., 2002, ApJ, 564, 974
in 't Zand, J. J. M., et al., 2000, A&A, 357, 520
in 't Zand, J. J. M., et al., 2002, A&A, 390, 597
in 't Zand, J. J. M., Miller, J. M., Oosterbroek, T., & Parmar, A. N., 2002b, A&A, 394, 553
Zdziarski, A. A., Gierlinski, M., Mikolajewska, J., Wardzinski, G., Smith, D. M., Harmon, B. A., Kitamoto, S., 2004, MNRAS, 351, 791
Zhang, S. N,. Cui, W., & Chen, W., 1997, ApJ, 482, L155
Zimmerman, E. R., Narayan, R., McClintock, J. E., & Miller, J. M., 2005, ApJ, 618, 832

TABLE 1

Black Hole Binary Parameters

Source	M_{BH} $M_\odot$	M_C $M_\odot$	q	θ (deg.)	P_{orb} (hours)	Dist. (kpc)
4U 1543–475[a]	9(2)	3(1)	5(2)	21(1)	26.8(1)	8(1)
XTE J1550–564[b]	11(1)	1.3(1)	9(2)	50-80	37.2(2)	3–8
XTE J1650–500[c]	5(2)	0.3–0.7	∼10	∼50	7.6(2)	5–11
GRO J1655–40[d]	7.0(2)	2.3(1)	3.0(2)	77(8)	62.9(1)	3.2(9)
GX 339–4[e]	≥ 6	$\geq$0.8	$\geq$8	–	42.1(1)	8–15
Cygnus X-1[f]	10(5)	∼18	0.6(3)	~ 35	134.0(1)	2.5(5)

NOTE.—Fundamental parameters for the black hole binaries treated in this work are given above. These parameters were used as inputs to the "kerrbb" disk continuum model when fitting the X-ray spectra in this paper. Parameters listed with a wave-like mark are very uncertain and were not used to bound parameters in fits with the "kerrbb" model. Instead, those parameters floated freely in all fits. Please see Section 2 for additional details. [a] Parameters taken from Park et al. (2004). [b] Parameters taken from Orosz et al. (2002). [c] Parameters taken from Orosz et al. (2004). [d] Parameters taken from Orosz & Bailyn (1997) and Hjellming & Rupen (1995). [e] Parameters taken from Hynes et al. (2003, 2004) and Munoz-Darias, Casares, & Martinez-Pais (2008). [f] Parameters taken from Herrero et al. (1995).

TABLE 2

Fully Relativistic Spectral Fits

Source	a	i (deg.)	q	N_H (10^{21} cm^{-2})	Γ	R	log(ξ)	$N_{\rm refl.}$ (10^{-26})	$N_{\rm disk}$	$\dot{M}_{disk}$ (10^{18} g s^{-1})x	ν	χ^2/ν
4U 1543–475	0.3(1)	22_{-1}	$3.0^{+0.1}$	4.0	2.48(5)	$2.0_{-0.1}$	4.5(1)	3.88(5)	0.72(2)	1.62(2)	55	1.15
XTE J1550–564	0.76(1)	50^{+1}	$5.0_{-0.1}$	6.67(1)	1.79(1)	$2.0_{-0.1}$	3.86(2)	1.41(2)	0.23(1)	0.70(1)	1493	1.23
XTE J1650–500	0.79(1)	45(1)	4.9(1)	5.58(1)	1.97(1)	0.56(1)	3.80(4)	4.96(1)	49.5(5)	$0.007^{+0.005}_{-0.002}$	1853	1.10
GRO J1655–40	0.98(1)	69^{+1}	$5.0_{-0.1}$	20.5(5)	2.60(2)	0.18(2)	$4.3^{+0.2}_{-0.5}$	140(9)	0.25(4)	0.18(4)	61	0.91
GX 339–4	0.94(2)	29(2)	4.9(1)	5.7(1)	2.74(5)	$2.0_{-0.2}$	4.8(2)	1.6(2)	0.67(5)	1.09(3)	1816	1.54
SAX J1711.6–3808	$0.6^{+0.2}_{-0.4}$	43(5)	$3.0^{+0.1}$	25.8(7)	1.69(2)	0.25(1)	3.0(1)	6.5(2)	–	–	40	0.93
XTE J1908+094	0.75(9)	45(8)	$3.0^{+0.1}$	21.5(5)	1.89(7)	0.17(1)	3.0	9(1)	–	–	297	1.51
Cygnus X-1	0.05(1)	30(1)	$3.0^{+0.1}$	6.84(2)	2.74(1)	1.3(1)	3.5(1)	290(5)	0.31(2)	0.96(1)	3687	1.78

NOTE.—The parameters listed are derived from fits to our stellar-mass black hole spectra with a blurred CDID reflection model and the "kerrbb" continuum model. Spin values and inclinations in the blurred reflection and disk continuum models were linked. To employ the "kerrbb" model, a number of parameters must be fixed or constrained a priori (e.g. distance, black hole mass, disk atmosphere hardening factor, etc.); for each source, please see the text for related details. The mass accretion rate given avove is an "effective" mass accretion rate; see Li et al. (2005) for details. The errors listed above are 1σ statistical errors, derived using the "error" command in XSPEC. Symmetric errors are given in parentheses; where one digit appears in parentheses it is the error in the last digit of the parameter value. SAX J1711.6–3808 and XTE J1908+094 did not require disk continuum components.

TABLE 3

Spectral Fits with a Simple Disk Continuum

Source	a	i (deg.)	q	N_H (10^{21} cm^{-2})	Γ	R	log(ξ)	$N_{\rm refl.}$ (10^{-26})	kT (keV)	$N_{\rm disk}$ (10^3)	ν	χ^2/ν
4U 1543–475	$0.3^{+0.2}_{-0.3}$	22_{-1}	3.1(1)	4.0	2.50(5)	$2.0_{-0.1}$	4.5(1)	0.41(4)	0.55(1)	9.40(2)	55	1.17
XTE J1550–564	0.78(2)	50(1)	$5.0_{-0.1}$	6.70(1)	1.92(1)	1.1(1)	3.92(6)	2.08(1)	0.66(1)	1.04(1)	1496	1.20
XTE J1650–500	0.87(1)	47(1)	$5.0_{-0.1}$	5.30(1)	1.96(1)	0.62(2)	3.86(1)	4.05(1)	0.31(1)	49.4(1)	1855	1.10
GRO J1655–40	0.94(3)	70(1)	$4.1^{+0.3}_{-0.9}$	17.6(1)	2.64(1)	0.42(5)	3.2(2)	180(30)	1.55(1)	0.13(1)	61	0.68
SAX J1711.6–3808	$0.6^{+0.2}_{-0.4}$	43(5)	$3.0^{+0.1}$	25.8(7)	1.69(2)	0.25(1)	3.0(1)	6.5(2)	–	–	40	0.93
XTE J1908+094	0.75(9)	45(8)	$3.0^{+0.1}$	21.5(5)	1.89(7)	0.17(1)	3.0	9(1)	–	–	297	1.51
Cygnus X-1	$0.00^{+0.05}$	24(1)	$3.0^{+0.1}$	6.80(1)	2.79(1)	0.93(5)	3.9(1)	170(01)	0.42(1)	43.0(1)	3689	2.01

NOTE.— The parameters listed are derived from fits to our stellar-mass black hole spectra with a blurred CDID reflection model and the "kerrbb" continuum model. The simple "diskbb" disk continuum model was used; this model does not measure spin directly and has only two variable parameters (temperature and flux). Please see the text for details on each source and spectrum. Fits to GX 339–4 using this disk continuum are detailed in Miller et al. (2008). The errors listed above are 1σ statistical errors, derived using the "error" command in XSPEC. Symmetric errors are given in parentheses; where one digit appears in parentheses it is the error in the last digit of the parameter value. SAX J1711.6–3808 and XTE J1908+094 did not require disk continuum components; values from Table 2 are repeated here to enable comparisons.